Quantitative simulation of a resonant tunneling diode

R. Chris Bowen,[a] Gerhard Klimeck, and Roger K. Lake
Central Research Laboratories, Texas Instruments Incorporated, Dallas, Texas 75265

William R. Frensley
Eric Jonsson School of Engineering and Computer Science, University of Texas at Dallas, Richardson, Texas 75083-0688

Ted Moise
Central Research Laboratories, Texas Instruments Incorporated, Dallas, Texas 75265

(Received 19 September 1996; accepted for publication 31 October 1996)

Quantitative simulation of an InGaAs/InAlAs resonant tunneling diode is obtained by relaxing three of the most widely employed assumptions in the simulation of quantum devices. These are the single band effective mass model (parabolic bands), Thomas-Fermi charge screening, and the Esaki-Tsu 1D integral approximation for current density. The breakdown of each of these assumptions is examined by comparing to the full quantum mechanical calculations of self-consistent quantum charge in a multiband basis explicitly including the transverse momentum. [S0021-8979(97)08503-4]

I. INTRODUCTION

Three of the most widely invoked assumptions in the simulation of resonant tunneling diodes are the use of effective-mass band structure models,[1–3] Thomas-Fermi charge screening,[4,5] and the Esaki-Tsu current density formula.[1,5–7] These assumptions greatly reduce the computational effort required to obtain a result. However, these assumptions also significantly restrict the number of structures which can be simulated quantitatively. Previous work has shown significant differences between simulations which invoke effective-mass and multiband bandstructure models.[4,5,8–11] Likewise, it has been shown that the Esaki-Tsu current density formula leads to unphysical IV features in many resonant tunneling diodes (RTDs).[12–15] The importance of quantum charge self-consistency has been examined in numerous articles.[3,16] However, simulations which relax all of these assumptions have not yet been presented and experimentally verified. In this work we examine the shortcomings of these assumptions systematically. When all of these assumptions are relaxed we arrive at a quantitative agreement with experiment.

We fabricated, measured and simulated the lattice matched InGaAs/InAlAs structure illustrated in Fig. 1. The area of the measured device is 12.2 μm^2. A measured extrinsic resistance of 10.1 Ω has been included in all simulated IV curves. The calculated zero bias conduction band edge and density of states for this structure are shown in Fig. 2. Though this device appears rather ordinary we shall show that quantitative agreement requires multiband bandstructure models, Hartree charge screening, and numerical integration over the transverse momentum in the current density calculation.

The conduction peak of this RTD occurs when a localized state in the emitter notch region is aligned with the well state. The density of states in the RTD for this bias condition is illustrated in Fig. 3. In order to simulate electron injection from the notch state we employ generalized boundary conditions which allow us to inject from both continuum and quasi-bound states in the contacts.[3,17] An optical potential of 6.6 meV is used in the leads to model the broadening of emitter quasi-bound states by scattering. The effect of incoherent scattering in the device is not included explicitly in the simulations presented here. Generally, the loss of phase coherence induced by inelastic scattering acts to reduce the peak current and increase the valley current. In the high current density, room temperature RTDs that we have examined we have found that broadening of emitter quasi-bound states and band structure effects account for most of the valley current. The effects of inelastic scattering are significant for low current density and/or low temperature RTDs.[18]

II. SINGLE BAND VERSUS MULTIBAND MODELS

Simulated and experimental IV curves for the InGaAs/InAlAs RTD are shown in Fig. 4. The simulations differ only in the band structure model used. The dot-dashed curve employs the single band effective mass model while the dashed curve uses the ten band nearest neighbor $sp3s^*$ model.[19] Effective masses, band offsets, and $sp3s^*$ parameters are provided in Table I. The single band model predicts a peak current that is a factor of 3 lower than experiment. Also, the second turn-on is predicted to occur at a much higher applied bias than experiment. Both of these inaccuracies are due to the fact that the single band effective-mass model does not incorporate real and imaginary band non-parabolicity.

The delayed second turn-on predicted by the single band model is due to the assumption that real bands are parabolic. In Fig. 5 the conduction bands and corresponding resonance energies for a typical RTD are illustrated. Resonances occur when the electron wavelength is a half integer multiple of the well width (Fig. 5). The resonance locations are given by the energies corresponding to these wavelengths on the energy dispersion relationship. Band non-parabolicity reduces the dispersion for a given value of k. Therefore, the single band model, which is roughly parabolic, significantly overpredicts

[a]Electronic mail: cbowen@spdc.ti.com

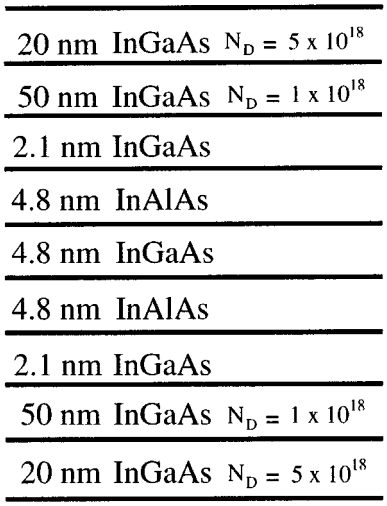

FIG. 1. Lattice-matched InGaAs/InAlAs RTD stack grown on InP substrate.

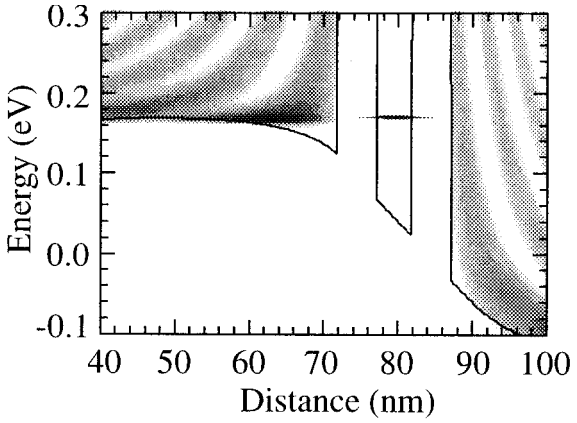

FIG. 3. Calculated conduction band edge and density of states for the InGaAs/InAlAs RTD for an applied bias of 0.3 V. A localized state residing in the emitter notch is aligned with the ground well resonance. The peak current of this RTD occurs when these states are strongly coupled.

the excited state resonance energy. Numerically calculated resonance energies for the InGaAs/InAlAs RTD are illustrated in Fig. 6.[20] The energy of the single band excited state resonance is over predicted by 106 meV. This explains the over prediction of the second turn-on voltage when using the single band model.

In the single band model imaginary bands are also parabolic (approach infinity as $E \rightarrow -\infty$). However, imaginary bands in semiconductors connect a pair of real bands rendering them highly non-parabolic. In Fig. 7 we show the complex band structure of a typical semiconductor for both single and ten band models. Note that the imaginary band in the full band model wraps back to the Γ-point ($k=0$) at the valence band edge. This is precisely what occurs in semiconductors. If one considers tunneling through a barrier at midgap, it is apparent that the single band model will predict an imaginary value of k which is larger than the prediction of the full band model. The imaginary value of k corresponds to the exponential decay constant in the barrier. The effect is that the single band model predicts the barrier to be more opaque to quantum tunneling than reality. Resonance widths predicted by the single band model will be smaller than reality resulting in lower predicted tunneling currents.

The ground state resonance widths in the InGaAs/InAlAs RTD predicted by the single and ten band models are 15.1 and 67.9 μeV, respectively. In Fig. 8 the transmission coefficients corresponding to the ground state resonance are plotted for the single band and ten band models. We see that the integral of the transmission coefficient for the single band model is significantly less than for the ten band model. This explains the difference in peak current predicted by the single and ten band models.

III. THOMAS-FERMI VERSUS HARTREE SCREENING

In this section we shall relax the assumption of Thomas-Fermi (local) charge screening. In much of the theoretical work on RTDs, the electron charge in the well region is assumed to be zero and Thomas-Fermi screening is assumed in the emitter and collector regions.[4,5] We should remark that

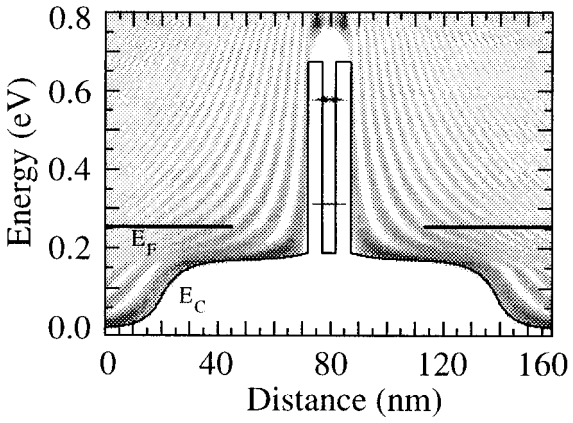

FIG. 2. Calculated conduction band edge and density of states for the InGaAs/InAlAs RTD at zero bias. The density of states is represented in gray scale. Darker gray scale represents larger state density.

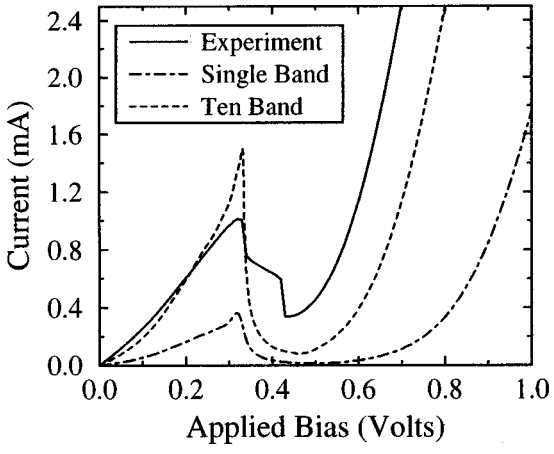

FIG. 4. Comparison between simulated and measured InGaAs/InAlAs RTD IV curves. Solid line is experiment, dot-dashed line is a single band simulation, and the dashed line incorporates the $sp3s^*$ band structure model.

TABLE I. Band structure model parameters. All parameters (except m^*) are in units of eV.

Parameter	InGaAs	InAlAs
m_Γ^*	0.0421	0.0770
E_G^Γ	0.771	1.491
E_c^Γ	0.000	0.504
$E(sa)$	−9.53777	−8.87382
$E(pa)$	0.98520	0.72863
$E(s^*a)$	7.95520	7.22917
$E(sc)$	−2.60209	−2.01908
$E(pc)$	3.64021	3.43956
$E(s^*c)$	6.72130	6.51716
$V(sa,sc)$	−5.89687	−5.78201
$V(sa,pc)$	3.80836	4.26641
$V(s^*a,pc)$	4.06793	3.78029
$V(pa,sa)$	6.50162	6.74933
$V(pa,s^*c)$	5.31514	6.01704
$V(x,x)$	1.89376	1.85814
$V(x,y)$	4.61063	4.67184

these assumptions have proven to be good for many RTDs. However, in order to obtain quantitative agreement with experiment the effects of quantization in the emitter notch and charge in the well must be taken into account. In Fig. 9 we compare the curves obtained using Thomas-Fermi and Hartree self-consistent potentials. When compared with the experimental curve, the Hartree calculation exhibits several improvements over the Thomas-Fermi calculation. Both the shape of the initial turn-on and the second turn-on voltage are closer to the experimental result. The existence of the anomalous spike in both simulations is a consequence of the 1D integral approximation used to calculate current. This assumption is relaxed in the following section.

In Fig. 10 the conduction band profiles and resonance energies for both the Hartree and Thomas-Fermi potentials are illustrated for an applied bias of 0.27 V. In the emitter notch the energy of the Hartree band profile is lower than that of the Thomas-Fermi profile. This is due to state quantization (i.e., lower density of states) in the emitter notch. In the well the energy of the Hartree band profile is larger than that of the Thomas-Fermi profile. This is due to electron charge residing in the ground state well resonance. The peak current of this device occurs when the emitter notch state is aligned with well state. Inspection of the resonance levels in

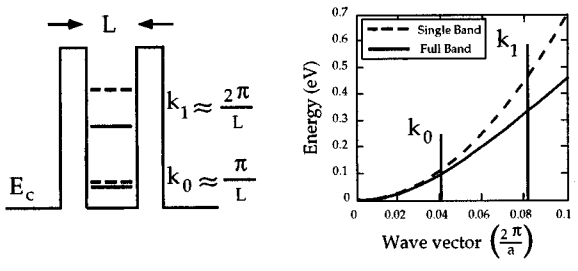

FIG. 5. (Right) Band structure of a typical III-V semiconductor predicted by single and full band models. (Left) Approximate resonant energies predicted by these band structure models in a typical RTD structure. The non-parabolicity of the conduction band acts to significantly reduce the excited state resonance energy level.

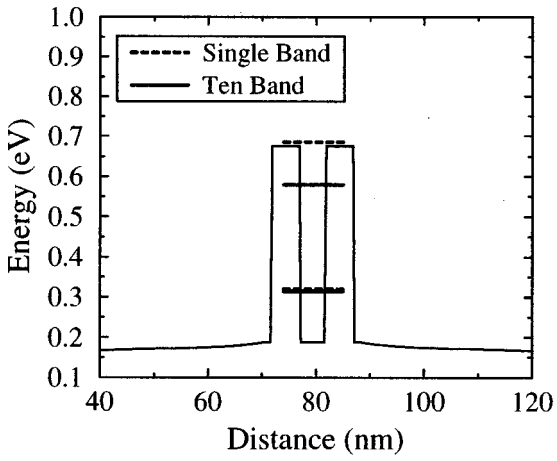

FIG. 6. Numerically calculated resonance energies for the InGaAs/InAlAs RTD using single and ten band models. No voltage is applied. The single band resonances are $E_0 = 319$ meV and $E_1 = 685$ meV and the ten band resonances are $E_0 = 314$ meV and $E_0 = 579$ meV. The single band model significantly over predicts the excited state resonance energy. This accounts for the higher second turn-on voltage predicted by the single band model.

Fig. 10 reveal that the peak current using Hartree potentials should occur at a larger applied bias. Indeed, this effect is manifested in the IV curve of Fig. 9.

In Fig. 11 the conduction band profiles and resonance energies for Hartree and Thomas-Fermi simulations at 0.7 V are shown. In this case the energy of the Hartree band profile is lower than that of the Thomas-Fermi profile in both the emitter notch and well regions. The reason for this is that there is very little charge in the well. There is no source for electrons to fill the ground well resonance and the excited well resonance is above the emitter Fermi level. This fact, along with quantization in the emitter notch, explains the lower energy profile for the Hartree simulation. The second turn-on of this device occurs via conduction through the excited well resonance. The Hartree calculation predicts a

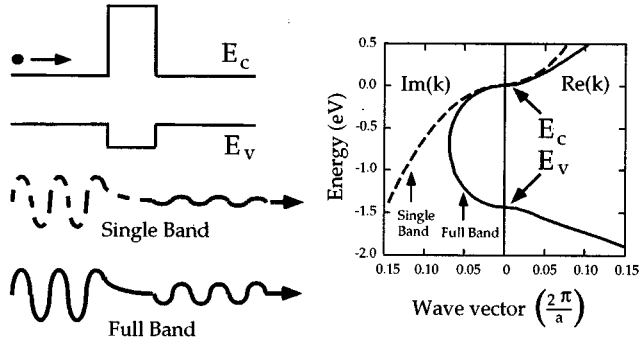

FIG. 7. (Right) Complex band structure of a typical III-V semiconductor for single band and full band models. Imaginary wave vectors are plotted on the left, real wave vectors are plotted on the right. The magnitude of the imaginary wave vector corresponds to the wave function decay constant. (Left) Illustration of barrier wave functions computed using single band and full band models (the barrier material corresponds to the complex band structure). The non-parabolicity of the imaginary band predicted by the full band model results in a larger tunneling amplitude.

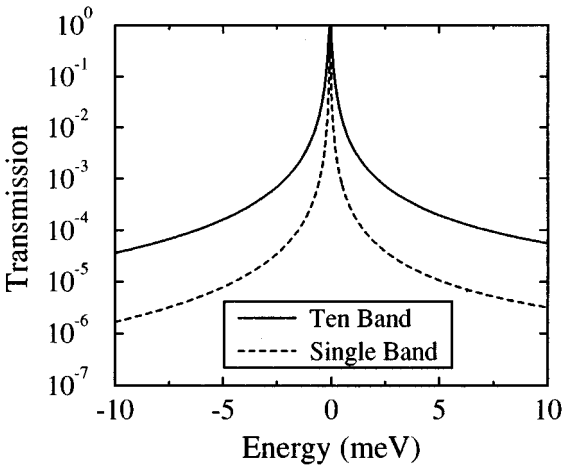

FIG. 8. Transmission coefficients vs energy for the ground state resonance using single and ten band models. The energy axis is normalized to the resonant energy. The resonance widths calculated by the single and ten band models are 15.1 and 67.9 μeV, respectively. This accounts for the low peak current density predicted by the single band model.

lower energy for this state and therefore a lower second turn-on voltage as illustrated in Fig. 9. The discontinuity in the Hartree IV curve at 0.44 V is due to the discharging of the ground well state. Since we do not include inelastic scattering in this simulation, this transition occurs rather abruptly. We should remark that the similar transition in the measurement is probably due to a power supply oscillation in the negative differential resistance (NDR) region. The similarity between theory and experiment in the appearance of this feature is only coincidental.

IV. ESAKI-TSU FORMULA VERSUS NUMERICAL TRANSVERSE INTEGRATION

In the pioneering work of Esaki and Tsu, a separation of variables approximation was invoked to reduce the current density formula to a one-dimensional integral.[7] Assuming axial symmetry about the direction of transport, the current density is expressed as follows:

$$J(V)=\frac{2q}{(2\pi)^2\hbar}\int\int [f_E(E,V) - f_C(E,V)]T(E,\mathbf{k},V)dEd\mathbf{k}, \tag{1}$$

where f_E and f_C are the Fermi-Dirac functions in the emitter and collector, $T(E,\mathbf{k},V)$ is the transmission coefficient, E is total energy, and $\mathbf{k}$ is the transverse momentum. Esaki and Tsu assume that the transverse momentum and energy variables are separable and invoke a parabolic transverse dispersion relationship.

$$T(E,\mathbf{k},V)\rightarrow T(E-E_t,0,V), \tag{2}$$

$$E_t=\frac{\hbar^2\mathbf{k}^2}{2m^*_{\text{emitter}}}. \tag{3}$$

The current density may then be expressed in terms of a one-dimensional integral over $\tilde{E}=E-E_t$,[7]

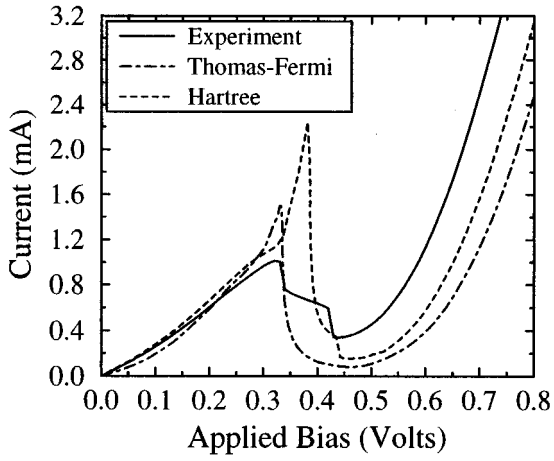

FIG. 9. Comparison between simulated and measured InGaAs/InAlAs RTD IV curves. Solid line is experiment and the dot-dashed line is an $sp3s^*$ simulation using Thomas-Fermi self-consistent potentials. The dashed line incorporates $sp3s^*$ and Hartree self-consistent potentials.

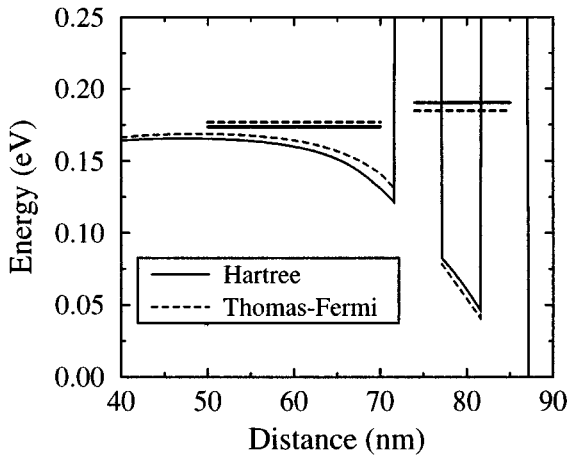

FIG. 10. Conduction band profiles and resonance energies for Thomas-Fermi and Hartree self-consistent potentials at an applied bias of 0.27 V.

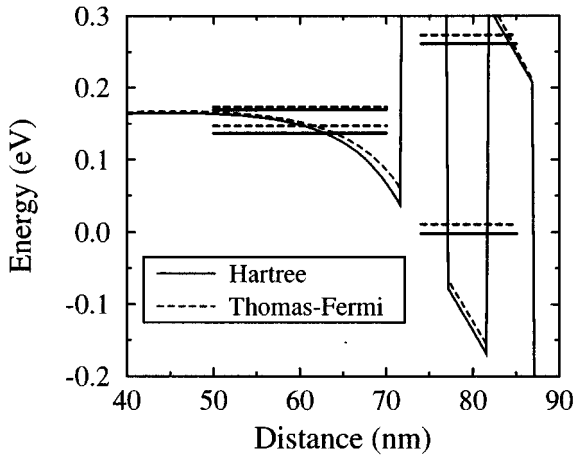

FIG. 11. Conduction band profiles and resonance energies for Thomas-Fermi and Hartree self-consistent potentials at an applied bias of 0.7 V.

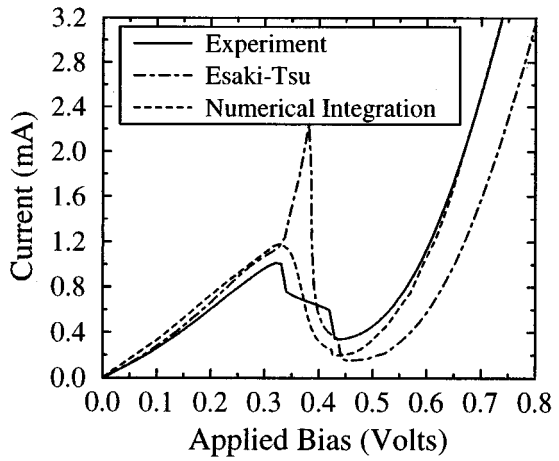

FIG. 12. Comparison between simulated and measured InGaAs/InAlAs RTD IV curves. Solid line is experiment and the dot-dashed line is an $sp3s^*$ simulation using Hartree self-consistent potentials. The dashed line incorporates $sp3s^*$, Hartree potentials, and numerical integration over the transverse momentum.

$$J(V)=\frac{qm^*_{\text{emitter}}kT}{2\pi^2\hbar^3}\int T(\widetilde{E},V) \times\ln\left(\frac{1+\exp[(E_F-\widetilde{E})/kT]}{1+\exp[(E_F-\widetilde{E}-qV)/kT]}\right)d\widetilde{E}. \tag{4}$$

This is perhaps the most widely invoked assumption in the simulation of RTDs. However, the implementation of this assumption can often lead to unphysical results.[13–15] Specifically, in any device in which multiple subbands are coupled, an unphysical spike can occur in the IV curve. Such a spike is readily noticeable in all of the simulated curves in the preceding sections. In Fig. 12 we compare simulations using Eqs. (1) and (4) with experiment. We see that when the separation of variables assumption is relaxed this unphysical spike vanishes. It is also apparent that the second turn-on of the device is simulated correctly and quantitative agreement with experiment is achieved. The peak current is slightly over predicted while the valley current is slightly under predicted. This is consistent with the fact that this simulation does not explicitly include scattering.

We shall now discuss the breakdown of the Esaki-Tsu formula for RTD simulation. When the separation of variables assumption is invoked, we implicitly assume that the transverse dispersion relationship of all the band edges *and* subbands are identical. In heterostructures, this is clearly not the case since different materials possess different dispersion relationships. However, if one considers the effect of this approximation on only the band edges, it really is not all that bad. In a standard RTD structure two materials are present, one for the well and another for the barrier. In the transverse direction, the band edges of both of these materials move up approximately quadratically as a function of **k**. The only difference is the quadratic prefactor which is proportional to $1/m^*$. The net result is that the barrier height of the RTD changes slightly as a function of **k**.

The breakdown of the separation of variables approximation occurs due to differences in subband transverse dispersion relationships. If realistic, non-parabolic band structure models are used, the transverse dispersion of different subbands can be significantly different. The transverse dispersion of a subband is related to the energy (with respect to the band edge) of that subband. Because of non-parabolicity, higher energy subbands will possess a smaller transverse curvature. The transverse dispersion is therefore dependent on the nature of the confining potential.

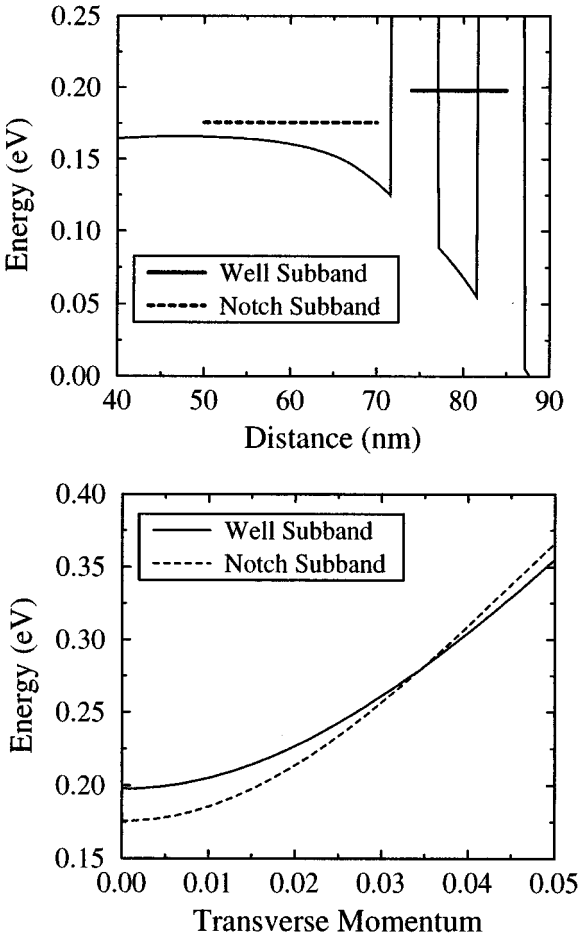

FIG. 13. Emitter notch and well subbands for an applied bias of 0.25 V. (Top) Spatial location of subbands at $\mathbf{k}=\mathbf{0}$. (Bottom) Subband energy vs transverse momentum in units of $2\pi/a$. The curvature of the emitter subband is larger than the well subband. Therefore the subbands are strongly coupled at non-zero transverse momentum.

In the case of the InGaAs/InAlAs RTD, the peak current occurs when a subband in the emitter notch is aligned with the well subband (see Fig. 3). The energy (with respect to the band edge) of the emitter notch subband is significantly smaller than the well subband. Therefore the curvature of the emitter notch subband should be larger than that of the well subband. In Figs. 13 and 14 these subbands are illustrated for applied biases of 0.25 and 0.30 V, respectively. The subbands are calculated using an efficient resonance finding algorithm.[20] In these figures it is clear that the emitter subband possesses a larger curvature. The result of this is that the emitter notch and well subband alignment occurs over a range of biases and transverse momentum.[21]

When the Esaki-Tsu formula is invoked, the curvatures

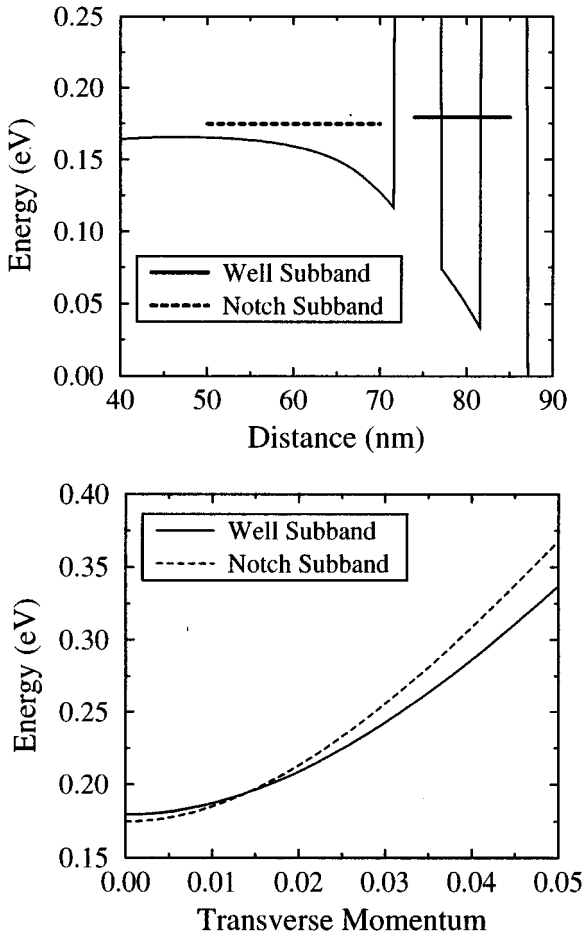

FIG. 14. Emitter notch and well subbands for an applied bias of 0.30 V. (Top) Spatial location of subbands at **k=0**. (Bottom) Subband energy vs transverse momentum in units of $2\pi/a$. The curvature of the emitter subband is larger than the well subband. Therefore the subbands are strongly coupled at non-zero transverse momentum.

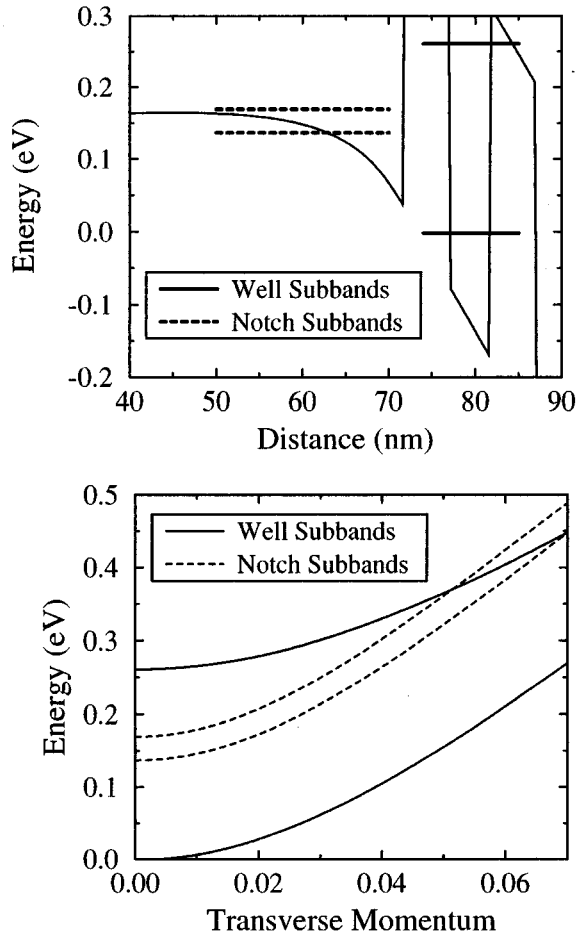

FIG. 16. Emitter notch and well subbands for an applied bias of 0.70 V. Top: Spatial location of subbands at **k=0**. Bottom: Subband energy vs transverse momentum in units of $2\pi/a$. The curvature of the emitter subbands are larger than the well subbands. Therefore the subbands are strongly coupled at non-zero transverse momentum.

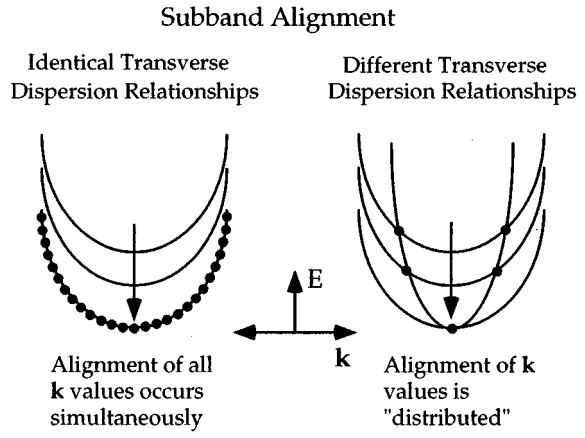

FIG. 15. Illustration of the alignment of two subbands possessing identical (left) and different (right) dispersion relationships. In the case of identical dispersions, the alignment of the two subbands occurs simultaneously for all momenta at one bias. In the case of different dispersions, the alignment is distributed over different values of **k** and biases. The one-dimensional integral approximation assumes that all subbands possess identical dispersion relationships. This results in current density spikes for structures in which a subband alignment takes place.

of these subbands are assumed to be identical. Thus, the subband lineup occurs for all transverse momentum simultaneously at one bias. This is graphically illustrated in Fig. 15. The result is the anomalous enhancement in Fig. 12 of the current at the bias (0.38 V) in which this alignment occurs.

Numerical integration over the transverse momentum is also necessary to quantitatively simulate the second turn-on of the InGaAs/InAlAs RTD. In this structure the second turn-on occurs when the excited notch subband couples with the excited well subband. The interaction between these subbands for an applied bias of 0.7 V is illustrated in Fig. 16. We see here that these subbands are much more strongly coupled for non-zero transverse momentum. The Esaki-Tsu formula only comprehends the strength of the subband coupling at $\mathbf{k}=0$. Thus, the second turn-on voltage predicted by the Esaki-Tsu formula is over predicted.

V. CONCLUSIONS

We have demonstrated quantitative simulation of an InGaAs/InAlAs RTD. This was achieved by relaxing three of the most widely applied assumptions in the simulation of quantum devices: single band models, Thomas-Fermi charge

screening, and the Esaki-Tsu current density formula. Full band structure models are required to incorporate non-parabolicity of both real and imaginary bands. Incorporation of band non-parabolicity is required to calculate the correct resonant energies and spectral widths. Hartree charge screening provides the correct electrostatic potential and numerical integration over the transverse momentum is necessary to simulate subband alignment.

ACKNOWLEDGMENTS

The authors gratefully acknowledge Tim Boykin for many helpful discussions and supplying the $sp3s^*$ parameters for InGaAs and InAlAs.

[1] D. Landlheer and G. C. Aers, Superlattices Microstruct. **7**, 17 (1990).
[2] J. Chen, G. Chen, C. H. Yang, and R. A. Wilson, J. Appl. Phys. **70**, 3131 (1991).
[3] G. Klimeck, R. Lake, R. C. Bowen, W. R. Frensley, and T. Moise, Appl. Phys. Lett. **67**, 2539 (1995).
[4] D. Z. Y. Ting, E. T. Yu, and T. C. McGill, Phys. Rev. B **45**, 3583 (1992).
[5] T. B. Boykin, J. P. A. van der Wagt, and J. S. Harris, Phys. Rev. B **43**, 4777 (1991).
[6] W. R. Frensley, *Heterostructures and Quantum Devices* (Academic, New York, 1994), pp. 273–303.
[7] R. Tsu and L. Esaki, Appl. Phys. Lett. **22**, 562 (1973).
[8] J. Schulman and Y. C. Chang, Phys. Rev. B **31**, 2056 (1985).
[9] D. Y. K. Ko and J. C. Inkson, Semicond. Sci. Technol. Rev. **3**, 791 (1988).
[10] K. V. Rouseau, K. L. Wang, and J. N. Schulman, Appl. Phys. Lett. **54**, 1342 (1989).
[11] T. B. Boykin and J. S. Harris, J. Appl. Phys. **72**, 988 (1992).
[12] T. B. Boykin, R. E. Carnahan, and R. J. Higgins, Phys. Rev. B **48**, 14232 (1993).
[13] T. B. Boykin, R. E. Carnahan, and K. P. Martin, Phys. Rev. B **51**, 2273 (1995).
[14] T. B. Boykin, Phys. Rev. B **51**, 4289 (1995).
[15] T. B. Boykin, J. Appl. Phys. **78**, 6818 (1995).
[16] M. Cahay, M. J. McLennan, S. Datta, and M. S. Lundstrom, Appl. Phys. Lett. **50**, 612 (1987).
[17] R. Lake, G. Klimeck, R. Chris Bowen, and D. Ovanovic, J. Appl. Phys. (submitted).
[18] R. Lake, G. Klimeck, R. Chris Bowen, C. Fernando, M. Leng. T. Moise, and Y. C. Kao, Superlattices Microstruct. **20**, 279 (1996).
[19] P. Vogl, H. P. Hjalmarson, and J. D. Dow, J. Phys. Chem. Solids **44**, 365 (1983).
[20] R. Chris Bowen, W. R. Frensley, G. Klimeck, and R. K. Lake, Phys. Rev. B **52**, 2754 (1995).
[21] H. Ohno, E. E. Mendez, and W. I. Wang, Appl. Phys. Lett. **56**, 1793 (1990).